Time-Resolved Spectrum of Light Reflected from Laser-Produced Plasmas

J. A. Tarvin and R. J. Schroeder
KMS Fusion, Inc., Ann Arbor, Michigan 48106
(Received 10 October 1980)

The time-dependent spectrum of 1.053-μm light reflected from spherical targets has been measured for intensities between 0.4×10^{15} and 10×10^{15} W/cm^2. The spectra are primarily shifted to the blue and are consistent with a Doppler-shift model. When compared with hydrodynamic code simulations, they place restraints on models for heat transport and suprathermal electron transport.

PACS numbers: 52.25.Ps, 52.25.Fi, 52.40.Db

The spectrum of light reflected from a laser plasma contains copious information about the laser-target interaction. However, spectra which are not time resolved[1-4] are difficult to interpret because a spectrum can change significantly in 50 ps or less. Time-resolved measurements of reflected spectra[5,6] have already been made with low-intensity pulses preceding the main laser pulses. The prepulses provided large volumes of preformed plasma and the observed red shifts were attributed to stimulated Brillouin scattering. In this Letter, we report measurements of the time-dependent spectrum of light reflected from spherical glass shells uniformly irradiated at a wavelength of 1.053 μm at intensities between 0.4×10^{15} and 10×10^{15} W/cm^2.

In these experiments, the incident laser light is focused onto the target by a pair of $f/0.2$ ellipsoidal mirrors.[7] The focus of each mirror is slightly behind the center of the target so that the entire target surface is illuminated. Light reflected from the target passes back through the illumination system and is partially transmitted through a dielectric turning mirror. This light is focused onto the input slit of a 0.5-m Ebert grating spectrograph at $f/50$. To achieve 10-ps resolution with a 590 groove/mm grating, we introduce an internal aperture 4.5 mm wide in the spectrograph. The output of the spectrograph is optically coupled to the input slit of a streak camera[8] with the light spectrally dispersed along the slit. The spectrograph-camera combination has a resolution of 15 ps and 3.5 Å.

The laser pulse width of 500 ps is obtained by coherently stacking five 100-ps pulses with 100 ps between pulses. The rise time of the resulting pulse is 30 ps and the power is nearly constant during the central 400 ps of the pulse. The energy arriving before the onset of the main pulse is sufficiently low that no plasma is observed in holographic interferograms taken 125 ps before the leading edge of the pulse. The intensity on target is changed by varying the laser power between 0.1 and 0.8 TW and the target diameter between 50 and 90 μm.

The spectrum for an intensity of 6.6×10^{15} W/cm^2 is shown in Fig. 1, where the incident wavelength λ_0 is indicated by a dot on the left and a streak on the right. The zero of the time scale has been set arbitrarily at the beginning of the reflected pulse, but, since the reflected pulse is about 500 ps long, the 250-ps point corresponds to the center of the incident pulse. The rapid variation of reflected power with time is probably due to coherent effects in the collection optics.[9] At a given time, the spectrum has considerable structure which can only be due to physical processes at the target. Turner and Goldman[6] observed fine structure in their spectra and they suggested that the peaks were harmonically related. The peaks in this spectrum do not appear to be harmonics.

What is unusual about this spectrum is the presence of a large blue shift. Previous measurements[2-6] have, with one exception,[1] been shifted to the red. In *all* cases, the shift has been interpreted as the result of stimulated Brillouin scattering (SBS), but, even with SBS, it is difficult

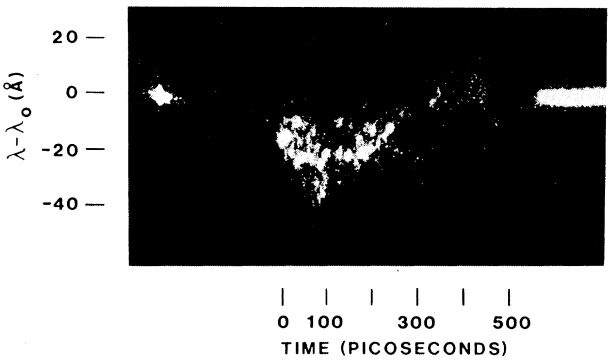

FIG. 1. Time-resolved spectrum at 6.6×10^{15} W/cm^2, with incident wavelength markers.

to understand how red shifts can be observed from solid targets.[10] We will show that, at least in this case, a different interpretation is applicable.

To analyze the spectra quantitatively, we have measured the extent of each spectrum as a function of time. Three spectra, analyzed this way, are plotted in Fig. 2. Each bar in a spectrum indicates the range of wavelength over which the exposure of the streak photograph is visible to the eye. The spectra are shifted to the blue by 10 to 20 Å initially and return to the incident wavelength after 200 to 300 ps. The magnitude of the maximum blue shift increases slowly with intensity as does the apparent linewidth.

The initial shifts in the spectra are close to the Doppler shifts which would be expected for light reflecting from the expanding plasma. Since our optical system provides illumination of the target at normal incidence, light is reflected at the critical surface, where the plasma frequency is equal to the laser frequency ω_0. The Doppler shift can be calculated by evaluating the phase integral

$$P = 2k_0 r_r - 2\int_{r_c}^{r_r} k_0 n\, dr = 2k_0 r_c + 2k_0 \int_{r_c}^{r_r} (1-n)\, dr. \quad (1)$$

Here, n is the index of refraction, r_r is a stationary reference point outside the plasma, r_c is the radius of the critical surface, and k_0 is the vacuum wave number of the incident light $2\pi/\lambda_0$. The frequency shift in the reflected light is given by[11]

$$\omega - \omega_0 = \frac{dP}{dt} = 2k_0 \dot{r}_c + 2k_0 \frac{d}{dt}\int_{r_c}^{r_r} (1-n)\, dr. \quad (2)$$

The first term on the right-hand side contains the effect of critical surface motion and the second term, variation of the plasma profile.[11] The phase integral can also be calculated by integrating the measured frequency shift as a function of time:

$$P(t) = \int_0^t (\omega - \omega_0)\, dt + 2k_0 r_{c0}. \quad (3)$$

Here r_{c0} is the initial radius of the target. It is particularly useful to view the spectra in terms of the phase integral because its time dependence is closely related to that of the critical radius, which is sensitive to energy transport in the target. The phase integrals derived from the smooth curves of Figs. 2(a) and 2(b) are plotted as solid curves in Fig. 3.

To verify that the Doppler-shift model is consistent with our spectra we have measured the critical surface trajectory for laser intensities near 1.5×10^{15} W/cm^2 by imaging the second harmonic ($2\omega_0$) emission from the critical surface as a function of time. Previous measurements

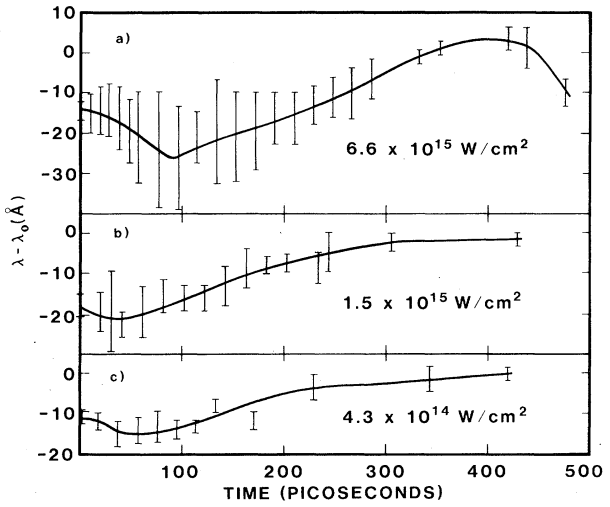

FIG. 2. Analyzed spectra. The length of a bar at a given time in a spectrum is the visible extent of the spectrum in the streak record at that time. Part (a) was derived from Fig. 1. The curves are guides to the eye.

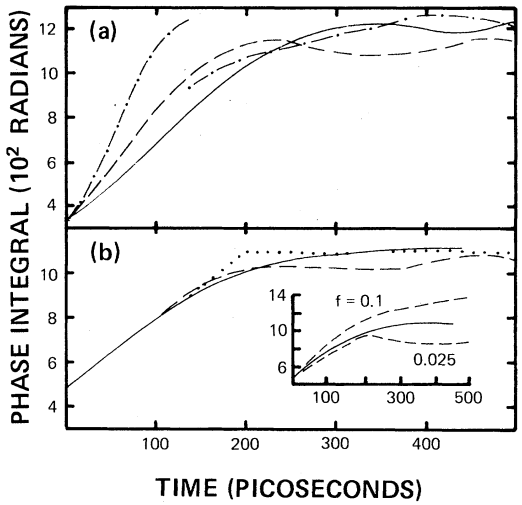

FIG. 3. Phase integrals for spectra of Figs. 2(a) and 2(b). Solid curves are derived from the spectra and Eq. (3). The dotted curve in (b) is estimated from direct measurements of the critical surface trajectory. Dashed curves result from code simulations which use Eq. (1) and a flux limiter, $f = 0.05$. The dot-dashed line in (a) shows the effect of changing suprathermal electron transport. The inset depicts the effect of varying the flux limit parameter.

have shown that the critical surface can move as fast as 3×10^7 cm/s at this intensity.[12-14] We find that the critical surface expands at a velocity of $2\pm0.5\times10^7$ cm/s for the first 150 ps and then slows down so that it is nearly stationary after 250 ps. The phase integral can be estimated from this information if the relative size of the two terms on the right-hand side of Eq. (2) is known. Our simulations, which are discussed below, indicate that the second term is 30% as large as the first. The dotted line in Fig. 3(b) is the estimate from the $2\omega_0$ measurement. Although it shows less detail and has a greater uncertainty, the $2\omega_0$ measurement agrees well with the spectrum.

To study energy transport in the target, we have simulated the experiments with our hydrodynamics code TRHYD.[15] Since the phase integral can be calculated accurately from Eq. (1) only if r_c and the density near r_c vary smoothly with time, we have used a version[16] of the code which inserts fine spatial zones near the critical surface. The code includes the effects of inverse bremsstrahlung absorption, ponderomotive force, and stimulated Brillouin scattering. Thermal flux is limited to $\frac{3}{2}fn_e\theta_e c_s/3$, where n_e and θ_e are the density and temperature of thermal electrons and c_s is the electron sound speed, $(5\theta_e/3m_e)^{1/2}$. In addition, resonance absorption is modeled by putting 28% of the laser energy reaching the critical surface in the suprathermal electron (STE) group. This fraction is chosen so that the code matches the measured absorption, which varied from 34% at the lowest intensity to 27% at the highest. The STE temperature is calculated from the laser intensity and the thermal electron temperature at the critical surface.[17] STE transport is modeled by depositing the resonantly absorbed energy in the region from the outer surface of the target to a point one STE mean free path inside the critical surface. For this calculation, the mean free path for energy deposition is the geometric mean of the mean free paths for electron-electron and electron-ion collisions because the electron-ion mean free path is shorter and only the electron-electron collisions transfer energy. Since fast electrons produced by resonance absorption move down the density gradient initially, many of them never get inside the critical surface.[18] The simulations account for this asymmetry by depositing resonantly absorbed energy uniformly per unit mass outside the critical surface while depositing only one-fourth as much energy per unit mass inside.

The simulations show that stimulated Brillouin scattering is limited to a few percent of the incident energy by large gradients of density and velocity outside the critical surface and that inverse bremsstrahlung absorption is also limited to a few percent. The best agreement between the data and the phase integral calculated from Eq. (1) occurs for a flux limiter of $f=0.05$. Those calculations are shown as dashed lines in Fig. 3. The simulations match the data somewhat better at lower intensities; but, at all intensities, they reproduce the qualitative features of the data—a linearly increasing phase integral during the first 200 ps and a nearly constant integral thereafter.

Early in the laser pulse, the motion of the critical surface is most sensitive to the modeling of STE transport. If resonantly absorbed energy is deposited uniformly per unit mass over the whole region of deposition, the electron temperature is made too high inside the critical surface. The result of this overestimate is shown as a dot-dashed line in Fig. 3(a). The critical surface expands so rapidly that the density profile develops a local maximum just inside the critical surface. Mass flow from the interior of the target is insufficient to maintain the local maximum, which eventually falls below critical density, and the critical surface jumps inward. The data show no sign of this discontinuity.

Late in the laser pulse, there is more mass outside the critical surface, and so less STE energy is deposited inside the critical surface and the phase integral is less strongly affected by modeling of STE transport. Since energy must now be transported inside the critical surface by thermal conduction, flux limitation becomes important. The inset in Fig. 3(b) shows how the phase integral varies when the flux limiter is increased or decreased from the best value. A weaker flux limiter ($f=0.1$) causes the critical surface to continue expanding, while a more stringent limiter causes a contraction.

While the mean shift of the time-resolved spectrum is consistent with this Doppler-shift model, the model makes no direct predictions about the time dependence of the spectral width. If, as we might guess, different parts of the critical surface move with different velocities at any particular time, the spectrum will contain a range of wavelengths which depends upon the range of velocities. Another mechanism for broadening the spectrum involves the illumination of the target. Some of the laser light (especially near the target equator) is not normal to the target sur-

face. This light is reflected from points outside the critical surface and experiences a range of Doppler shifts.

The time-resolved spectra reported here are found to agree in detail with a simple Doppler-shift model. As a result, they give detailed information on the critical surface trajectory, which depends on the transport of heat and of suprathermal electrons inside the critical surface.

We are grateful to J. R. Albritton, R. L. Berger, G. Charatis, F. J. Mayer, D. Mitrovich, D. C. Slater, T. Speziale, and M. A. True for valuable discussions. This work was supported by the U. S. Department of Energy under Contract No. DE-AC08-78DP40030.

[1]D. W. Phillion, W. L. Kruer, and V. C. Rupert, Phys. Rev. Lett. 39, 1529 (1977).

[2]M. D. Rosen, D. W. Phillion, V. C. Rupert, W. C. Mead, W. L. Kruer, J. J. Thomson, H. N. Kornblum, V. W. Slivinsky, G. J. Caporaso, M. J. Boyle, and K. G. Tirsell, Phys. Fluids 22, 2020 (1979).

[3]F. J. Mayer, G. E. Busch, C. M. Kinzer, and K. G. Estabrook, Phys. Rev. Lett. 44, 1498 (1980).

[4]R. E. Turner and L. M. Goldman, Phys. Rev. Lett. 44, 400 (1980).

[5]B. H. Ripin, J. M. McMahon, E. A. McLean, W. M. Manheimer, and J. A. Stamper, Phys. Rev. Lett. 33, 634 (1974).

[6]R. E. Turner and L. M. Goldman, Phys. Fluids 24, 184 (1981).

[7]C. E. Thomas, Appl. Opt. 14, 1267 (1975).

[8]Imacon 675, manufactured by Hadland Photonics, Ltd.

[9]C. E. Thomas, private communication.

[10]C. J. Randall, J. J. Thompson, and K. G. Estabrook, Phys. Rev. Lett. 43, 924 (1979).

[11]T. Dewandre, J. R. Albritton, and E. A. Williams, Phys. Fluids 24, 528 (1981).

[12]T. A. Leonard and R. A. Cover, J. Appl. Phys. 50, 3241 (1979).

[13]S. Jackel, J. Albritton, and E. Goldman, Phys. Rev. Lett. 35, 514 (1975).

[14]S. Jackel, B. Perry, and M. Lubin, Phys. Rev. Lett. 37, 95 (1976).

[15]K. A. Brueckner and S. Jorna, Rev. Mod. Phys. 46, 325 (1974).

[16]L. V. Powers and D. J. Tanner, Bull. Am. Phys. Soc. 24, 1104 (1979).

[17]K. Estabrook, J. Harte, and D. Bailey, Laser Program Annual Report—1978, Lawrence Livermore Laboratory Report No. UCRL-50021-78 (unpublished), p. 3–31.

[18]J. R. Albritton, I. B. Bernstein, E. J. Valeo, and E. A. Williams, Phys. Rev. Lett. 39, 1536 (1977).

Nonlinear Stabilization of the Farley-Buneman Instability by Strong $\vec{E}\times\vec{B}$ Turbulence in a Plasma

M. J. Keskinen

Plasma Physics Division, Naval Research Laboratory, Washington, D. C. 20375

(Received 4 May 1981)

It is shown that through nonlinear model coupling processes long-wavelength, low-frequency strong $\vec{E}\times\vec{B}$ turbulence can stabilize short-wavelength, high-frequency Farley-Buneman modes in a weakly ionized low-pressure convecting plasma. Favorable comparisons are made with experimental observations.

PACS numbers: 52.35.Ra

It is well known that in the absence of a magnetic field the two-stream instability can occur in a homogeneous plasma when the electron drift velocity with respect to the ions exceeds the electron thermal velocity.[1] Farley[2] and Buenman[2] have shown that, in the presence of a magnetic field, the electron drift velocity with respect to the ions has only to exceed the ion acoustic velocity c_s to generate unstable waves traveling perpendicular to the magnetic field. We will consider the nonlinear evolution of the Farley-Buneman instability in a low-β, weakly ionized, convecting plasma which is subjected to a magnetic field $B\hat{x}$, an electric field $E_0\hat{z}$, and a density gradient $(\partial n_0/\partial z)\hat{z}$. Differences in the collision frequencies ($\nu_i/\Omega_i \gtrsim 1$, $\nu_e/\Omega_e \ll 1$) of the ions and electrons with the background neutral gas result in the formation of a cross-field current $-J_0\hat{y}$ from the electron drift $\vec{V}_d = \vec{E}_0\times\vec{B}/B^2$. For weak currents J_0, long-wavelength field-aligned fluctuations in

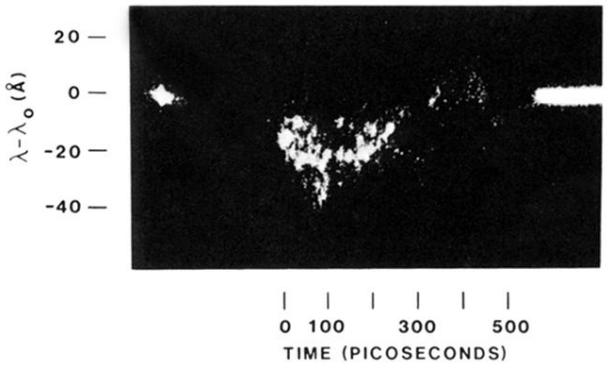

FIG. 1. Time-resolved spectrum at 6.6×10^{15} W/cm^2, with incident wavelength markers.